Observer-Based Dynamic Control of an Underactuated Hand

Huang Hai [a,*], **Jiang Li** [b], **Pang Yong-jie** [a], **Shi Shi-cai** [b], **Tang Qi-rong** [c], **Yang Da-peng** [b] **and Liu Hong** [d]

[a] Key Laboratory of Science and Technology for National Defense of Autonomous Underwater Vehicle, Harbin Engineering University, Harbin 150001, P. R. China

[b] State Key Laboratory of Robotics and Systems, Harbin Institute of Technology, Harbin 150001, P. R. China

[c] University of Stuttgart, Pfaffenwaldring 9, 70569 Stuttgart, Germany

[d] Institute of Robotics and Mechatronics, German Aerospace Center, DLR, 82230 Wessling, Germany

Received 9 December 2008; accepted 2 April 2009

Abstract

The purpose of this paper was to construct a velocity observer based on the dynamic model and realize accurate dynamic curve and force control. Curve fitting with the observer obtained precise velocity signals. Compared with PID and factored moment methods, it decreased the fitting errors a lot and achieved ideal results. Compensated with the inverse dynamic equation, the force-based impedance control with the observer could not only realize accurate force tracking, but achieve finger dynamic control by the combination of curve fitting and force tracking. Furthermore, a static grasp model was established for appropriate force distribution. The finger could grasp slippery, fragile, comparatively heavy and large objects like an egg with only base joint torque and position sensors, which illustrated that the hand could accomplish difficult tasks by using the static grasp model and dynamic control.

Keywords

Underactuated, dynamic control, velocity observer, curve fitting, force control

1. Introduction

Research on the humanoid hand, widely recognized as the current challenge for robotics research, is attracting the interest of many worldwide research groups. Important efforts have been devoted to the objectives of developing humanoid hands

and impressive results have been achieved [1]. Highly integrated hands such as the Utah/MIT Hand, NASA Hand, DLR Hand, DLR-HIT Hand, GiFu Hand and Stanford/JPL Hand [2–8] have been developed.

Underactuation in a robotic hand has intriguing properties, such as simple architecture and fewer actuators than degrees of freedom (d.o.f.). These underactuated joints can be governed by passive elements like springs or mechanical limits, which leads to an automatic shape adaptation of one finger [9, 10]. Fruitful research has been accomplished from many institutes with regard to this aspect, such as the UB Hand, TBM Hand, Italian Hand, i-limb Hand and OTTOBOCK Hand [11–18]. They can fulfill ordinary tasks, and can be utilized by serving robots and handicapped persons.

However, precise curve and force control are troubled by the existence of passive elements and lack of velocity sensors. Complicated work can be difficult to accomplish due to the limited number of d.o.f.

Alternatively, a velocity observer could provide precise and reliable estimated velocity values in the robotic control areas [19–21]. Based on the hand dynamic and static model, this paper focuses on the dynamic control of a underactuated hand, in order to establish a velocity observer for accurate control of difficult tasks.

2. Model of Underactuated Fingers

2.1. Dynamic Model

In an underactuated finger, the actuation torque T_a is applied to the input of the finger and is transmitted to the phalanxes through a suitable mechanical design, e.g., four-bar linkages, pulleys and tendons, gears, etc. Since underactuated finger actuators have fewer d.o.f., passive elements are used to kinematically constrain the finger and ensure the shape-adaptation grasp of the finger. To this end, springs and mechanical limits are often used [22].

A typical underactuated hand (HIT-DLR Prosthetic Hand II) is illustrated in Fig. 1. Its finger is composed of three phalanxes i.e., proximal phalange, mid pha-

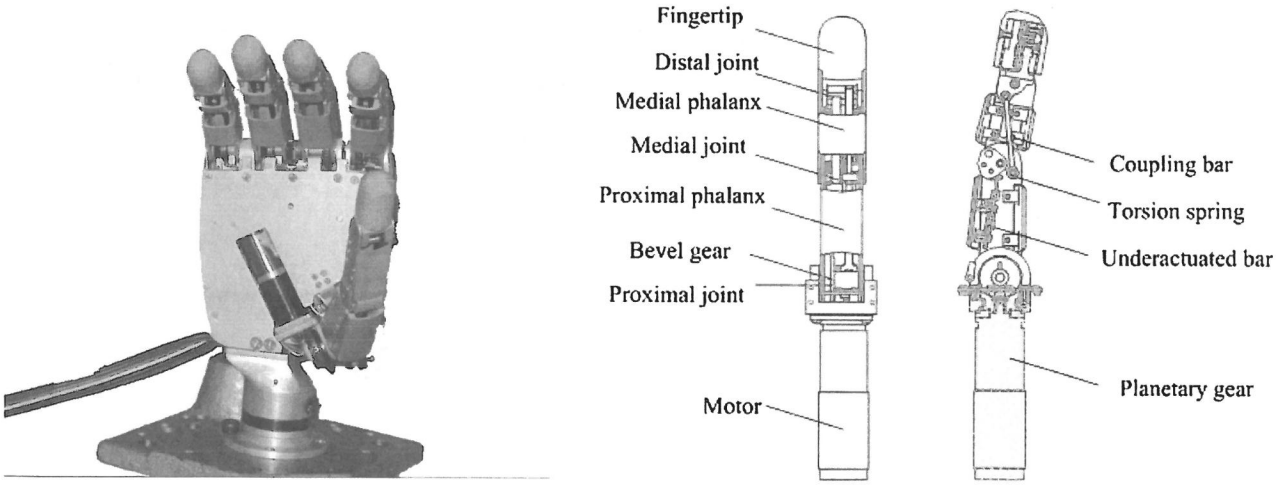

Figure 1. HIT-DLR Prosthetic Hand II and its finger mechanism.

lange and fingertip. Its base joint is actuated by a motor. A torsion spring is installed in its mid joint. It consisted of an underactuated four-bar in the proximal phalange and a 1:1 coupling four-bar in the mid phalange. A position and torque sensor are available at the base joint. Therefore, we obtained the dynamic model of the finger as:

$$M(q)\ddot{q} + C(q,\dot{q})\dot{q} + F\dot{q} + G(q) + T_{\mathrm{L}} = \tau. \tag{1}$$

Two links of its coupling bars group were fixed on the underactuated bars group. Thus, there were six independent angle variables in the finger. In the model, $M(q)$ is the 6×6 mass matrix of the finger, q is the 6×1 vector of linkages angles, $C(q,\dot{q})$ is the 6×1 vector of centrifugal and Coriolis terms, F is the 6×1 vector viscous and friction, $G(q)$ is the sum of the 6×1 vector of gravity and torsion spring terms, T_{L} is the external torque on the finger, and τ is the motor torque at the base joint. When the finger grasped in free space, $T_{\mathrm{L}} = 0$.

2.2. *Static Grasp Model*

In order to determine the configurations where the finger can apply forces to the object grasped, we shall proceed with a quasi-static modeling of the finger. The model will provide us with the relationship between the input actuator torque and the forces exerted on the object. Equating the input and the output virtual powers, we obtain:

$$T^{\mathrm{T}}\omega = F^{\mathrm{T}}V, \tag{2}$$

where T is the input torque vector exerted by the actuator and the spring (Fig. 2), ω is the corresponding velocity vector, F is the vector of contact forces and V is the velocity of the contact points projected onto the respective normal of the phalange. Contact forces are assumed to be normal to the phalanges and without friction. More precisely, we have:

$$T = \begin{bmatrix} T_0 \\ T_1 = -k_1(\theta_2 + \theta_{20}) \\ T_2 = 0 \end{bmatrix} \tag{3}$$

$$\omega = [\,\alpha_1 \quad \theta_2 \quad \theta_3\,]^{\mathrm{T}}, \quad F = [\,F_1 \quad F_2 \quad F_3\,]^{\mathrm{T}}, \quad V = [\,V_{\mathrm{c1y1}} \quad V_{\mathrm{c2y2}} \quad V_{\mathrm{c3y3}}\,]^{\mathrm{T}}. \tag{4}$$

The projected velocities of the contact points can be simply expressed as the product of a Jacobian matrix J_{v} and the derivatives of the phalanx joint coordinates which is a natural choice, i.e.,

$$\begin{bmatrix} V_{\mathrm{c1y1}} \\ V_{\mathrm{c2y2}} \\ V_{\mathrm{c3y3}} \end{bmatrix} = \begin{bmatrix} d_1 & 0 & 0 \\ l_1\cos\theta_2 & d_2 & 0 \\ l_1\cos(\theta_2+\theta_3) + l_2\cos\theta_3 + d_3 & l_2\cos\theta_3 + d_3 & d_3 \end{bmatrix} \begin{bmatrix} \dot{\theta}_1 \\ \dot{\theta}_2 \\ \dot{\theta}_3 \end{bmatrix},$$

where:

$$J_{\mathrm{v}} = \begin{bmatrix} d_1 & 0 & 0 \\ l_1\cos\theta_2 & d_2 & 0 \\ l_1\cos(\theta_2+\theta_3) + l_2\cos\theta_3 + d_3 & l_2\cos\theta_3 + d_3 & d_3 \end{bmatrix}.$$

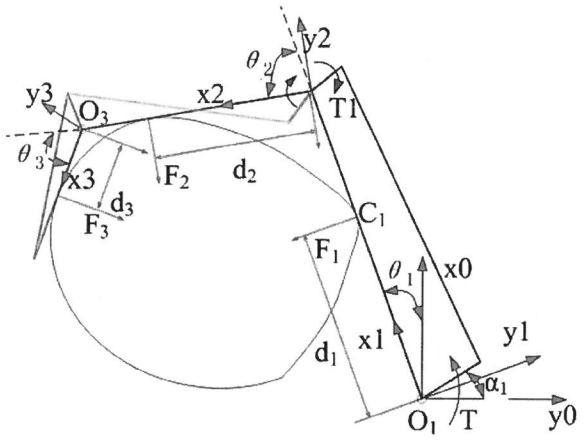

Figure 2. Static module of the finger.

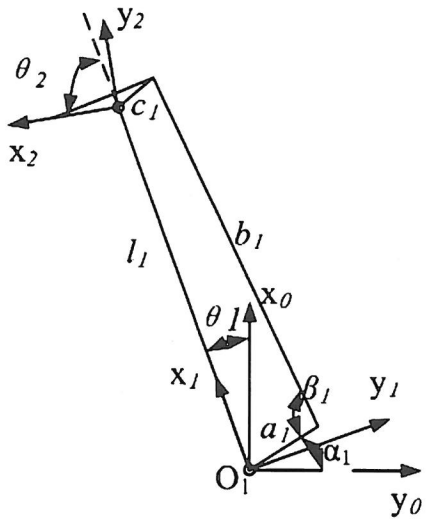

Figure 3. Sketch diagram of the four-bar linkages.

According to Fig. 3 the initial angles between a_1 and l_1, l_1 and c_1, and a_1 and y_0 are θ_0, α_0 and β_0, respectively. During grasping, link a_1 has turned α_1, while the proximal and mid phalanges turned θ_1 and θ_2, respectively; at that time the angles between a_1 and l_1, l_1 and c_1 are $\theta_0 + \theta_1 - \alpha_1$ and $\beta_0 + \theta_2$, respectively. We have:

$$a_1^2 + b_1^2 - 2a_1 b_1 \cos(\beta_1) = c_1^2 + l_1^2 - 2c_1 l_1 \cos(\beta_0 + \theta_2)$$

$$\begin{aligned} &a_1^2 + l_1^2 - 2a_1 l_1 \cos(\theta_1 + \theta_0 - \alpha_1) \\ &\quad = b_1^2 - 2c_1 b_1 \cos(\beta_2)\theta_0 + \theta_1 - \alpha_1 + \beta_0 + \theta_2 + \beta_1 + \beta_1 = 360^\circ \end{aligned}$$

$$\dot{\theta}_1 = \dot{\alpha}_1 - \frac{1 + \dfrac{\sin(\beta_0 + \theta_2)c_1 l_1}{b_1 a_1 \sqrt{1 - (b_1^2 + a_1^2 - c_1^2 + 2\cos(\beta_0 + \theta_2)c_1 l_1 - l_1^2)^2/(4b_1^2 c_1^2)}}}{1 + \dfrac{\sin(\theta_1 + \theta_0 - \alpha_1)a_1 l_1}{b_1 c_1 \sqrt{1 - (b_1^2 - a_1^2 + c_1^2 + 2\cos(\theta_1 + \theta_0 - \alpha_1)a_1 l_1 - l_1^2)^2/(4b_1^2 c_1^2)}}} \dot{\theta}_2. \tag{5}$$

The mid phalange and fingertip are 1:1 coupled, i.e., $\dot{\theta}_2 = \dot{\theta}_3$, and the mass ratio between the two is 7:3, and we have:

$$\begin{bmatrix} \dot{\theta}_1 \\ \dot{\theta}_2 \\ \dot{\theta}_3 \end{bmatrix} = \begin{bmatrix} 1 & -0.7A & -0.3A \\ 0 & 1 & 0 \\ 0 & 0 & 1 \end{bmatrix} \begin{bmatrix} \dot{\alpha}_1 \\ \dot{\theta}_2 \\ \dot{\theta}_3 \end{bmatrix},$$

where:

$$A = \frac{1 + \dfrac{\sin(\beta_0 + \theta_2) c_1 l_1}{b_1 a_1 \sqrt{1 - (b_1^2 + a_1^2 - c_1^2 + 2\cos(\beta_0 + \theta_2) c_1 l_1 - l_1^2)^2 / (4 b_1^2 c_1^2)}}}{1 + \dfrac{\sin(\theta_1 + \theta_0 - \alpha_1) a_1 l_1}{b_1 c_1 \sqrt{1 - (b_1^2 - a_1^2 + c_1^2 + 2\cos(\theta_1 + \theta_0 - \alpha_1) a_1 l_1 - l_1^2)^2 / (4 b_1^2 c_1^2)}}}.$$

According to (2)–(5), we have:

$$V = J_v J_\omega \begin{bmatrix} \dot{\alpha}_1 \\ \dot{\theta}_2 \\ \dot{\theta}_3 \end{bmatrix},$$

where:

$$J_\omega = \begin{bmatrix} 1 & -0.7A & -0.3A \\ 0 & 1 & 0 \\ 0 & 0 & 1 \end{bmatrix}.$$

J_v and J_ω are nonsingular matrices due to $d_1 \neq 0$ and $d_1 d_2 d_3 \neq 0$. We have:

$$F = J_v^{-\mathrm{T}} J_\omega^{-\mathrm{T}} T,$$

i.e.:

$$F_1 = \frac{T_0}{d_1} - \frac{0.7 A T_0 (l_1 \cos\theta_2 + d_2)}{d_1 d_2} + \frac{k_1 (l_1 \cos\theta_2 + d_2)(\theta_2 + \theta_{20})}{d_1 d_2} + \frac{0.3 A T_0 l_1 [l_2 \cos\theta_2 \cos\theta_3 + d_3 \cos\theta_2 - d_2 \cos(\theta_2 + \theta_3)]}{d_1 d_2 d_3}$$

$$F_2 = \frac{0.7 A T_0}{d_2} - \frac{0.3 A T_0 (l_2 \cos\theta_3 + d_3)}{d_2 d_3} - \frac{k_1 (\theta_2 + \theta_{20})}{d_2}$$

$$F_3 = \frac{0.3 A T_0}{d_3}.$$

Skipping the torque from the torsion spring, we obtain the static grasp mode:

$$\begin{cases} F_1 = \dfrac{T_0}{d_1} - \dfrac{0.7AT_0(l_1\cos\theta_2 + d_2)}{d_1 d_2} \\ \qquad + \dfrac{0.3AT_0 l_1[l_2\cos\theta_2\cos\theta_3 + d_3\cos\theta_2 - d_2\cos(\theta_2+\theta_3)]}{d_1 d_2 d_3} \\ F_2 = \dfrac{0.7AT_0}{d_2} - \dfrac{0.3AT_0(l_2\cos\theta_3 + d_3)}{d_2 d_3} - \dfrac{k_1(\theta_2+\theta_{20})}{d_2} \\ F_3 = \dfrac{0.3AT_0}{d_3}. \end{cases} \tag{6}$$

3. Dynamic Curve Fitting

3.1. Velocity Observer

Trajectory planning is an important stage in the kinematics analysis of finger model, since it is supposed to mimic the natural movements of the human finger.

The motion velocity can only be acquired from the position differential, which results in great errors. In this paper, the velocity observer will be brought forward in order to obtain precise and reliable velocity values of the finger's base joint.

Several properties of the finger dynamic equation are useful in the development of the proposed adaptive observer controller and these are summarized as:

Property 1. The manipulator inertia matrix is positive definite symmetric and bounded $m_{\mathrm{i}} \leqslant \|M(q)\| \leqslant m_{\mathrm{u}}$, where $m_{\mathrm{i}}, m_{\mathrm{u}} > 0, \forall q \in \Re^6$.

Property 2. $C(q,x)$ is bounded by $C(q,x) \leqslant m_{\mathrm{c}}\|x\|$, where $m_{\mathrm{c}} > 0$ is a positive constant.

Property 3. The matrix of Christoffel symbols, $C(q,x)$, satisfies $C(q,x)\xi = C(q,\xi)x$ for any $q, x, \xi \in \Re^5$.

Property 4. $\xi^{\mathrm{T}}(\dot{H}(q) - 2C(q,x))\xi = 0$ for any $\xi \in \Re^6$.

In the formulation of the adaptive finger velocity observer it is useful to reman-age (1) to give:

$$\dot{x} = M^{-1}(q)[\tau - C(q,x)x - Fx - G(q)], \tag{7}$$

where $x = \dot{q}$. This is a first-order equation in x where q is assumed to be known, τ is the input and x is the output. The proposed observer has a similar structure given by:

$$\dot{\hat{x}}_{\mathrm{a}} = \hat{M}^{-1}(q)[\tau - \hat{C}(q,\hat{x}_{\mathrm{a}})\hat{x}_{\mathrm{a}} - \hat{F}\hat{x}_{\mathrm{a}} - \hat{g}(q)] + K\tilde{x}_{\mathrm{a}}, \tag{8}$$

where $\hat{x}_{\mathrm{a}}$ is the observed velocity, $\tilde{x}_{\mathrm{a}} = x - \hat{x}_{\mathrm{a}}$ is the observer error, $K > 0$ is a diagonal gain matrix and $(\hat{*})$ denotes the estimate of $(*)$.

3.2. Controller

The proposed controller is a variation on the factored moment controller where the actual velocity is replaced by the velocity estimated by the observer. The controller is defined by the expression:

$$\tau = M(q)[\ddot{q}_d - K_d(\hat{x} - \dot{q}_d) - K_p\tilde{q}] + C(q, \hat{x}_a)\dot{q}_d + V\dot{q}_d + g(q). \tag{9}$$

The error dynamics is derived by subtracting the control torque (4) from (1) and using Properties 3 and 4. The result is given by:

$$\begin{aligned} M(q)\ddot{\tilde{q}} = &-[C(q, x) + M(q)K_d + V]\dot{\tilde{q}} \\ &- [C(q, \hat{x}_a) + M(q)K_d]\tilde{x} - M(q)K_p\tilde{q}, \end{aligned} \tag{10}$$

where $\tilde{q} = q - q_d$ is the position tracking error with desired position trajectory $q_d(t)$. The proportional and derivative gain matrices are K_p and K_d, respectively.

Theorem 1. *If* $\|\dot{q}\| \leqslant m_v, \forall t \geqslant 0$, *then* $\tilde{x}, \tilde{q}, \dot{\tilde{q}} \to 0$ *as* $t \to \infty$, *where* $\tilde{x}$ *belongs to the region of attraction defined by* $\Omega = \left\{\tilde{x} \in R : \|\tilde{x}\| < \left(\frac{\underline{\sigma} - m_e m_v}{m_c} - \frac{(K_d + m_e m_v + m_e m_c)}{\varepsilon^2 m_e}\right)\right\}$ *provided that* $K_d, K_v > 0$ *and* $\varepsilon > 0$ *are chosen such that* $K_d + K_v > \varepsilon^2(K_d + m_e m_v + m_e m_c)$ *and* $\underline{\sigma} > m_e\|\tilde{x}\| + m_e m_v + \frac{(K_d + m_e m_v + m_e m_c)}{4\varepsilon^2}$, *where* $K_v = \lambda_{\min}(V)$ *and* $m_e = \max \|\dot{q} - \dot{q}_d\|$.

Proof. Consider the Lyapunov function candidate:

$$v(t) = \frac{1}{2}e(t)^T P(q(t))e(t), \tag{11}$$

where $e^T = [\tilde{x}^T \quad \dot{\tilde{q}}^T \quad \tilde{q}^T]$. By using Property 1 and $K_p > 0$, we conclude that Lyapunov candidate function $v(t)$ satisfies:

$$\frac{1}{2}p_l\|e(t)\|^2 \leqslant v(t) \leqslant \frac{1}{2}p_u\|e(t)\|^2. \tag{12}$$

The time derivative of (11) is given by:

$$\begin{aligned} \dot{v} \leqslant &-(\underline{\sigma} - m_e m_v - m_e\|\tilde{x}\|)\|\tilde{x}\|^2 - (K_d + K_v)\|\dot{\tilde{q}}\|^2 \\ &+ (K_d + m_e m_v + m_e m_c)\|\tilde{x}\|\|\dot{\tilde{q}}\|, \end{aligned} \tag{13}$$

where (8), (10) and Property 4 are used. Now since:

$$(\varepsilon\|\dot{\tilde{q}}\|)^2 + \left(\frac{\|\tilde{x}\|}{\varepsilon}\right)^2 \geqslant (\varepsilon\|\dot{\tilde{q}}\|)\left(\frac{\|\tilde{x}\|}{\varepsilon}\right) = \|\dot{\tilde{q}}\|\|\tilde{x}\|,$$

(13) can be rewritten as:

$$\dot{v} \leqslant -\beta_1\|\tilde{x}\|^2 - \beta_2\|\dot{\tilde{q}}\|^2, \tag{14}$$

where $\beta_1 = \left(\underline{\sigma} - m_e m_v - m_e\|\tilde{x}\| - \frac{K_d + m_e m_v + m_e m_c}{4\varepsilon^2}\right)$, $\beta_2 = K_v - \varepsilon^2(K_d + m_e m_v + m_e m_c) + K_d$.

We can now fix an ε and choose K_d, to make β_2 as large as we need. Then for fixed K_d and ε, a proper K can be chosen so that $\underline{\sigma}$ is large enough to make $\beta_1 > 0$ whenever $\forall \tilde{x} \in \Omega$. It follows from (14) that inside the region Ω, $\dot{v} \equiv 0$ implies $\tilde{x} \equiv 0$. With these substitutions, (10) reduces to $\tilde{q} \equiv 0$. Consequently, by using the well-known Lasalle theorem, we conclude that $\tilde{q} \to 0$ as $t \to \infty$. Further, (14) implies that $v(t)$ is bounded and $\tilde{x}, \dot{\tilde{q}} \in L_2$. From (12), $\tilde{x}, \dot{\tilde{q}}, \tilde{q} \in L_\infty$, which in conjunction with (10) implies the boundness of $\ddot{\tilde{q}}$. The use of Barbalat's Lemma concludes that $\dot{\tilde{q}} \to 0$ as $t \to \infty$. Similarly, it can be shown that $\tilde{x} \to 0$, i.e., $\hat{x}(t) \to x(t)$ as $t \to \infty$.

4. Force Control

From (1) we can see that the external force cannot be measured directly by joint torque sensors. The measurement of base joint torque also includes inertia, centrifugal, Coriolis and gravitational forces of the links. If the finger moves at a very slow speed, the dynamic forces can be set to zero approximately, i.e., $M(q)\ddot{q} \approx 0, C(q, \dot{q}) \approx 0$. Therefore, if the gravity force is compensated in the whole workspace, at the equilibrium state the external force can be calculated as:

$$T_L \approx \tau - G(q). \tag{15}$$

The angles of the links can be calculated through the finger geometry, because it has only 1 active d.o.f. Using this control scheme we would be able to control the complete impedance property of a finger:

$$T_L = M_d(\ddot{q}_{br} - \ddot{q}) + B_d(\dot{q}_{br} - \dot{q}) + K_d(q_{br} - q), \tag{16}$$

where M_d, B_d and K_d are the desired target impedance parameters of the finger, and q_{br} is the reference angle of the base joint. In order to keep the target impedance, we can deduce the following motor output torque by introducing (16) into (1):

$$\begin{aligned} T = {} & M(\theta)\left(\ddot{\theta}_d - M_d^{-1}\left(T_L - B_d\delta\hat{\dot{\theta}} - K_d\delta\theta\right)\right) + V\left(\theta, \hat{\dot{\theta}}\right) \\ & + F\left(\theta, \hat{\dot{\theta}}, \operatorname{sign}\left(\hat{\dot{\theta}}\right)\right) + G(\theta) + T_L, \end{aligned} \tag{17}$$

where $\delta\dot{q} = \dot{q}_d - \hat{\dot{q}}$ and $\delta q = q_d - q$. This means with precise knowledge of finger dynamics and accurate sensors, we can achieve a perfect feedback linearization for driving torque calculation, and the finger will show the desired impedance parameters M_d, B_d and K_d to the environment. However, in reality, the finger dynamics is not known precisely, and the accuracy of the position and torque sensors is always affected by some noise. This means, practically, that it would be very difficult to realize a perfect linearization and, hence, the desired impedance parameters cannot be achieved. Alternatively, we can also introduce an explicit force control scheme, i.e., let:

$$T_d = M_d'\delta\hat{\dot{q}} + B_d'\delta\hat{q} + K_d'\delta q. \tag{18}$$

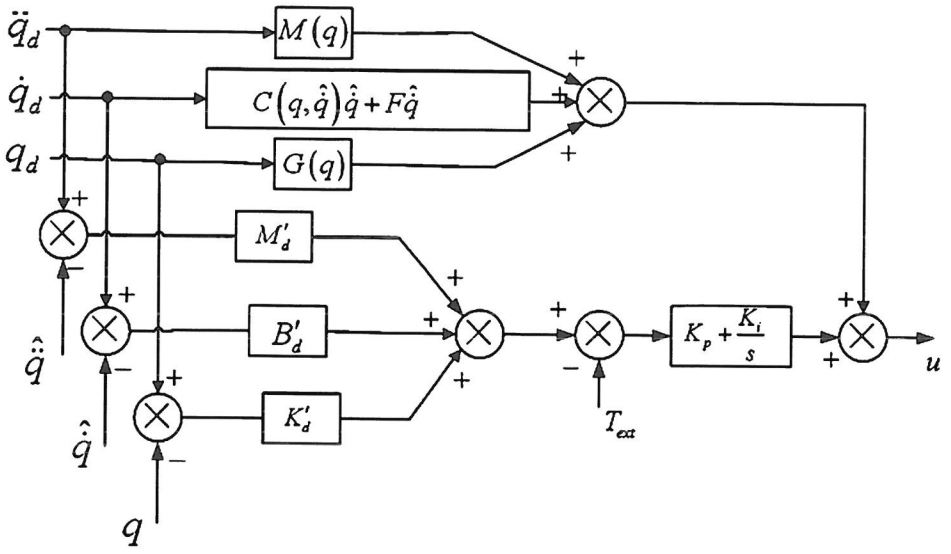

Figure 4. Strategy of the force-based impedance control system.

Let $T_e = T_d - T_{ext}$ be the error function. Now we can introduce a simple PI control scheme with z as input. If T_e converges to zero, the actual impedance parameters will converge to the desired values automatically. With the addition of the control signal from PI and estimated finger dynamics (1), we can build an impedance controller as shown in Fig. 4. In the steady state, all measured and desired velocity and acceleration values are zero. This shows that the value of the steady-state torque is the stiffness multiplied by the steady-state deformation δq and the fingertip behaves like a programmable spring.

5. Experiments

In Fig. 5 all phalanges of the finger grasped consistently over 0–36°, while the underactuated grasp worked over 37–55°; the finger stopped at 55°. The motion range of the base joint was 58° due to the object. Therefore, although PID (Fig. 5b) could realize accurate position control, it could not accomplish precise curve fitting without the algorithm for the underactated features. Based on the dynamic model from Section 2, the factored moment (Fig. 5c) curve fitting bettered PID control. However, the results were not ideal because the uncertain parameters such as inertia, damp, etc., were compensated for and the velocity could only be acquired through position differential. In comparison with the position differential, the observer increased the velocity acquisition (Fig. 5h). The adapted curve fitting with the observer made up the shortcomings without velocity sensors and the uncertain factors, reducing the tracing and velocity errors, and achieved ideal results.

Figures 6 and 7 illustrate the experimental results from force-based impedance control. According to the desired trajectory, the base joint should move at a constant linear speed of 45°/s. The desired trajectory would increase until 53.6° after the fingertip contacted with the object; at that time the grasp force would switch according to the desired force, which was acquired through the desired trajectory and impedance. Grasp force changed greatly at the impact point and reached its stable

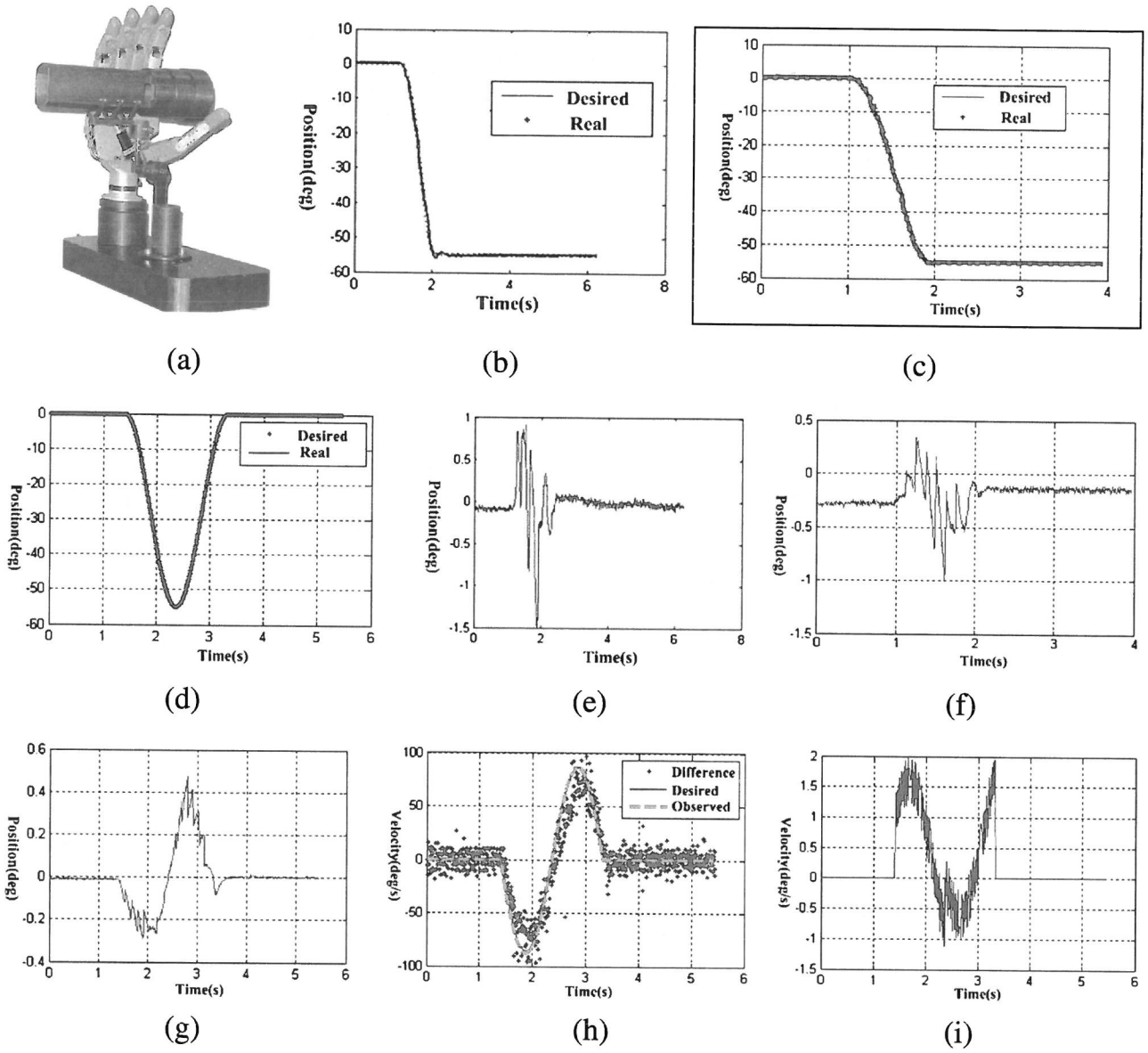

Figure 5. Dynamic curve fitting experimental results. (a) Experimental platform. (b) Fitting curve of PID control. (c) Fitting curve of factored moment. (d) Curve fitting with observer. (e) Fitting errors of PID. (f) Fitting errors of factored moment. (g) Fitting errors with observer. (h) Curves of velocity. (i) Velocity errors with observer.

state quickly. In Figs 6 and 7, iron and sponge objects were grasped, respectively. The implied desired force could be obtained though changing the desired trajectory instead of the desired impedance. Therefore, accurate force control could be achieved by using force-based impedance control. In the following experiment, the finger was going to grasp an egg by using force control (Section 4) and the static grasp model (Section 2). Stable and balanced forces should be provided because the egg is slippery, fragile, comparatively heavy and large. The closed force model including grasp forces and friction was established as in Fig. 8. Table 1 depicts the grasp force from each phalange. Thus, the torque from the base joint was 0.33 Nm, according to (6). According to the strategy from Fig. 4 , the torque of the base joint could be precisely controlled, the grasp forces were distributed consistent with Table 1 and the finger could grasp the egg successfully (Fig. 9). However, the egg

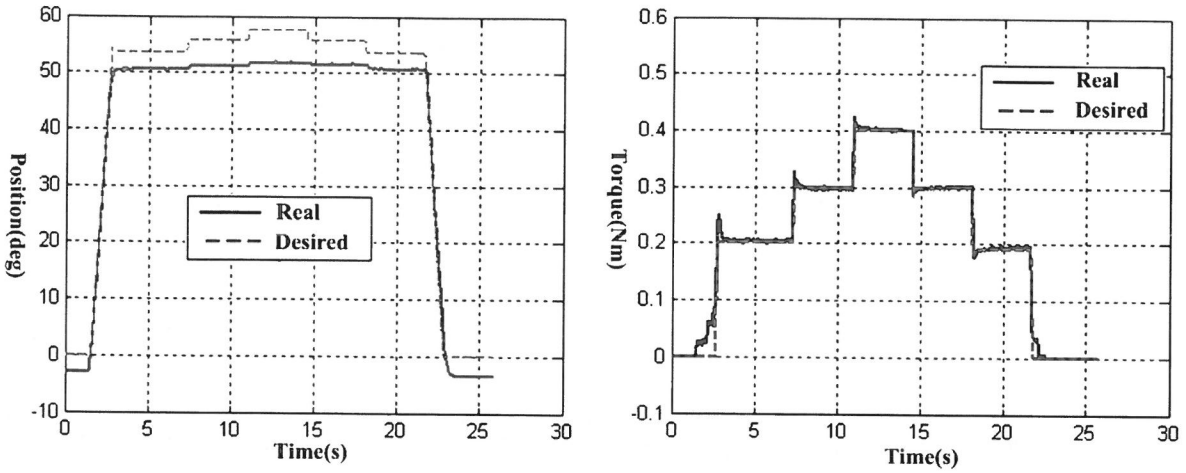

(a) (b)

Figure 6. Experimental results of joint torque tracking during grasping metal. (a) Position response of base joint. (b) Torque response of base joint.

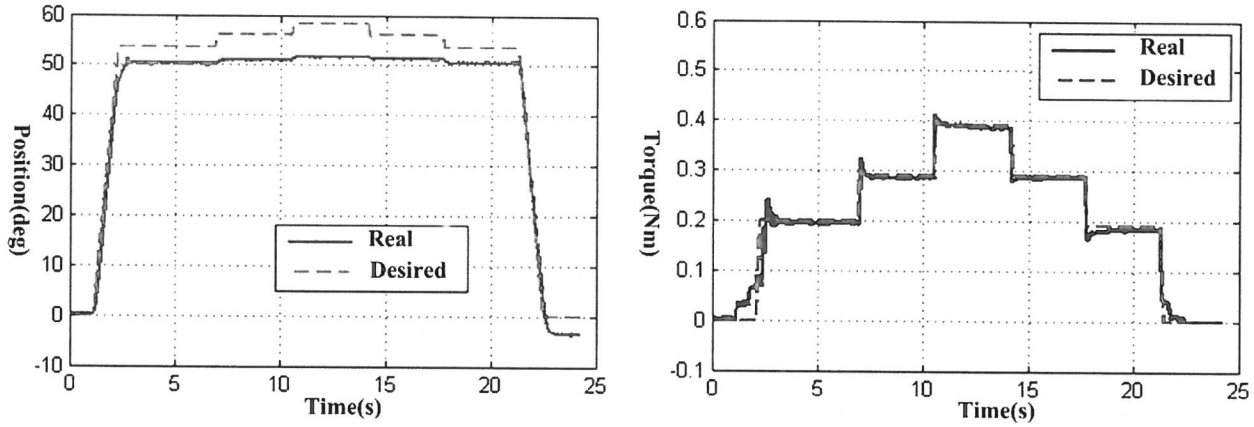

(a) (b)

Figure 7. Experimental results of joint torque tracking during grasping foam. (a) Position response of base joint. (b) Torque response of base joint.

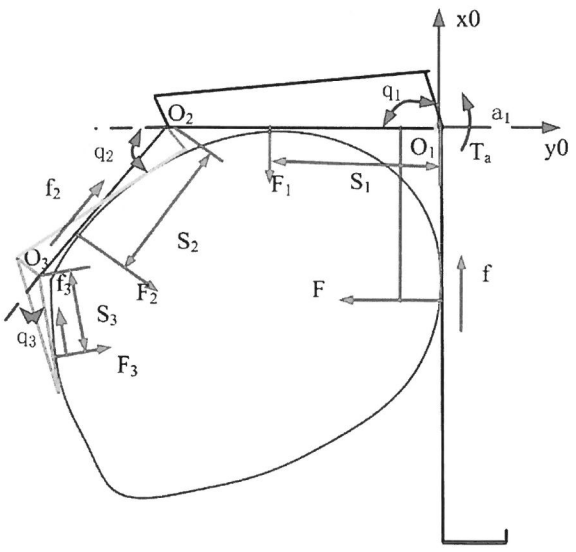

Figure 8. Closed force model of grasping an egg.

Table 1.
Grasp force of each phalange and relevant parameters during grasping an egg

	Proximal phalange	Mid phalange	Fingertip
Grasp force (N)	8.35	3.13	2.71
Position of joints (°)	90	36	36
Contact point from joints (mm)	28.6	16.6	14.4

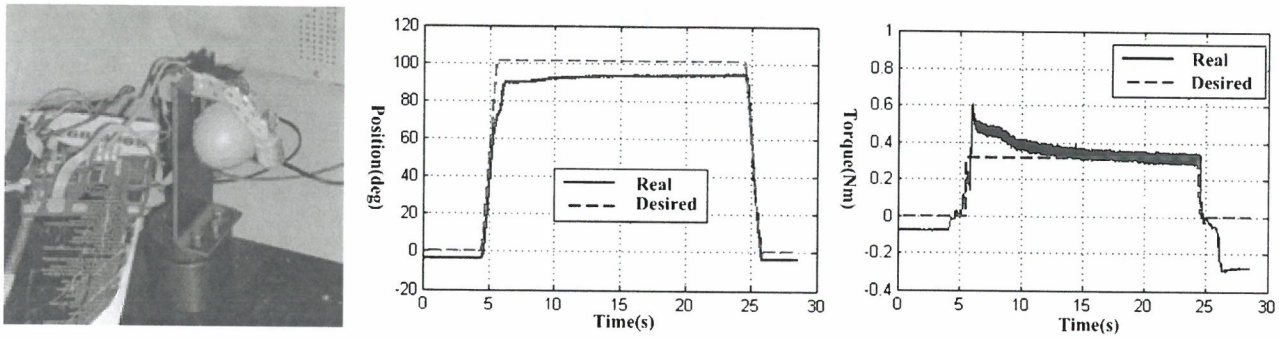

Figure 9. Experimental results during grasping an egg.

could be grasped simply through impedance control only at less than 20% success rate, according to repeated experiments. Therefore, the finger can grasp slippery, fragile, comparatively heavy and large objects like an egg with only the base joint torque sensor by providing an appropriate force distribution through the static grasp model.

6. Conclusions

Based on the dynamic model, the velocity observer was established and the curve fitting with the observer obtained precise velocity signals. In comparison with PID and factored moment methods, it greatly decreased the fitting errors and achieved ideal results. However, the force-based impedance control strategy was built by using a dynamic model.

The velocity observer was also used in impedance control. Compensated with the inverse dynamics equation, the force-based impedance control could not only realize accurate force tracking, but achieve finger dynamic control in the combination with curve fitting and force tracking. Furthermore, the static finger grasp model was established. Through appropriate force distribution, the finger could grasp slippery, fragile, comparatively heavy and large objects like an egg with only the base joint torque sensor, which illustrates that the hand can accomplish difficult tasks by using the static grasp model and dynamic control.

One of the greatest gaps between human beings and robots is that the former possess the capability of integrative reasoning, perception and action [23–25]. Future work will further improve the intelligent capability of the hand. The key step is to construct higher-level cognitive functions for the proposed work (e.g., a qualitative

representation to symbolize the hand task) in order to enable the hand to act and 'perceive' in dynamic, partially unknown and unpredictable environments.

Acknowledgements

This project is supported by National Science Foundation of China (50435040) and Program for Changjiang Scholars and Innovative Research Team in University (PCSIRT).

References

1. P. Dario, C. Laschi and M. C. Carrozza, An integrated approach for the design and development of a grasping and manipulation system in humanoid robotics, in: *Proc. IEEE Int. Conf. on Robotics and Automation*, Washington, DC, pp. 556–562 (2002).
2. A. Edsinger-Gonzales, Design of a compliant and force sensing hand for a humanoid robot, in: *Proc. Conf. on Intelligent Manipulation and Grasping*, Genova, pp. 291–295 (2004).
3. S. C. Jacobsen, E. K. Iversen, D. F. Knutti, R. T. Johnson and K. B. Biggers, Design of the UTAH/M. An integrated approach for the design and development of a grasping and manipulation system in humanoid robotics IT dextrous hand, in: *Proc. IEEE Int. Conf. on Robotics and Automation*, San Francisco, CA, pp. 1520–1532 (2001).
4. M. A. Diftler, R. Platt, C. J. Culbert, R. O. Ambrose and W. J. Bluethmann, Evolution of the NASA/DARPA robonaut control system, in: *Proc. IEEE Int. Conf. on Robotics and Automation*, Taipei, pp. 2543–2548 (2003).
5. T. Wimböck, C. Ott and G. Hirzinger, Impedance behaviors for two-handed manipulation: design and experiments, in: *Proc. IEEE Int. Conf. on Robotics and Automation*, Rome, pp. 4182–4187 (2007).
6. H. Liu, P. Meusel, N. Seitz, B. Willberg, G. Hirzinger, M. H. Jin, Y. W. Liu, R. Wei and Z. W. Xie, The modular multisensory DLR-HIT-Hand, *Mech. Mach. Theory* **42**, 612–625 (2007).
7. H. Kawasaki, T. Mouri and S. Ito, Toward next stage of kinetic humanoid hand, in: *Proc. World Automation Congr. 10th Int. Symp. on Robotics with Applications*, Seville, pp. 129–134 (2004).
8. C. S. Loucks, V. Johnson, P. Boissiere, G. Starr and J. Steele, Modeling and control of the Stanford/JPL hand, in: *Proc. Int. Conf. on Robotics and Automation*, Raleigh, NC, pp. 573–578 (1987).
9. B.-H. Kim and S. Hirai, Characterizing the dynamic deformation of soft fingertips and analyzing its significance for multi-fingered operations, in: *Proc. IEEE Int. Conf. on Robotics and Automation*, New Orleans, LA, pp. 2944–2950 (2004).
10. Y. Imai, A. Namiki, K. Hashimoto and M. Ishikawa, Dynamic active catching using a high-speed multifingered hand and a high-speed vision system, in: *Proc. IEEE Int. Conf. on Robotics and Automation*, New Orleans, LA, pp. 1849–1854 (2004).
11. P. H. Chappell and P. J. Kyberd, Prehensile control of a hand prosthesis by a microcontroller, *Biomed. Eng.* **13**, 363–369 (1991).
12. N. Dechev, W. L. Cleghorn and S. Naumann, Multiple finger, passive adaptive grasp prosthetic hand, *Mech. Mach. Theory* **36**, 1157–1173 (2001).
13. L. Zollo, S. Roccella, E. Guglielmelli, C. Carozza and P. Dario, Biomechatronic design and control of an anthropomorphic artificial hand for prosthetic and robotic applications, *IEEE/ASME Trans. Mechatron.* **12**, 418–429 (2007).
14. L. Lotti, P. Tiezzi and C. Melchiorri, Development of UB Hand 3, in: *Proc. IEEE Int. Conf. on Robotics and Automation*, Barcelona, pp. 4499–4503 (2005).

15. N. Chev, W. L. Cleghorn and S. Naumann, Multiple finger, passive adaptive grasp prosthetic hand[J], *Mech. Mach. Theory* **36**, 1157–1173 (2001).
16. L. Zollo, S. Roccella and R. Tucci, Biomechatronic design and control of an anthropomorphic artificial hand for prosthetics hand robotic applications, in: *Proc. Biorob2006*, Pisa, pp. 198–203 (2006).
17. http://www.touchbionics.com
18. http://www.ottobock.de
19. E. D. Engeberg, S. G. Meek and M. A. Minor, Hybrid force–velocity sliding mode control of a prosthetic hand, *IEEE Trans. Biomed. Eng.* **55**, 1572–1581 (2008).
20. D. Chwa, J. Y. Choi and S. G. Anavatti, Observer-based adaptive guidance law considering target uncertainties and control loop dynamics, *IEEE Trans. Control Syst. Technol.* **14**, 112–123 (2006).
21. S.-K. Kim, J.-H. Jeon, C.-H. Cho and J.-B. Ahn, Dynamic modeling and control of a grid-connected hybrid generation system with versatile power transfer, *IEEE Trans. Ind. Electron.* **55**, 1677–1688 (2008).
22. W. Schiehlen, A. Rukgauer and Th. Schirle, Force coupling *versus* differential algebraic description of constrained multibody systems, *Multibody Syst. Dyn.* **4**, 317–340 (2000).
23. H. Liu, A fuzzy qualitative framework for connecting robot qualitative and quantitative representations, *IEEE Trans. Fuzzy Syst.* **16**, 1522–1530 (2008).
24. H. Liu and G. M. Coghill, Fuzzy qualitative trigonometry, in: *Proc. IEEE Int. Conf. on Systems, Man and Cybernetics*, Maui, HI, pp. 1291–1296 (2005).
25. Q. Shen and R. Leitch, Fuzzy qualitative simulation, *IEEE Trans. Syst. Man, Cybernet.* **23**, 1038–1061 (1993).